



Synthesis and Characterization of Ag₂S Doped TiO₂ Nanocatalysts for the Photocatalytic Degradation of Methylene Blue Dye Under UV Light Irradiation

T. Arunkumar^a and M. Shanthi^{a*}

Department of chemistry, Annamalai University, Annamalai Nagar, India.

(Received: 04 February 2024

Revised: 11 March 2024

Accepted: 08 April 2024)

KEYWORDS

Ag₂S – TiO₂, MB dye, Photocatalyst, UV light, and operational parameters.

ABSTRACT:

The Ag₂S – TiO₂ nanocatalysts were effectively synthesized using the precipitation–thermal decomposition method. Characterization of the prepared catalyst was conducted through X-ray diffraction (XRD), Field emission scanning electron microscope (FE- SEM), Energy dispersive spectra (EDS), Ultra-violet diffuse reflectance spectra (UV- DRS), Photoluminescence (PL), and X-ray photoelectron spectroscopy (XPS) measurements. The photocatalytic activity of Ag₂S – TiO₂ was examined for the deterioration of Methylene blue (MB) dye in aqueous solution under UV-A light. Ag₂S – TiO₂ demonstrated superior effectiveness compared to other photocatalysts (ZnO, Ag₂S, TiO₂, etc.) at pH 7 for MB dye mineralization. The effect of operational parameters including photocatalyst amount, dye concentration, and initial pH on MB dye photomineralization was analyzed. Active species trapping revealed the significant roles of holes, electrons, hydroxyl radicals, and superoxide radicals in the photocatalytic deterioration of MB dye. A proposed mechanism for dye deterioration using Ag₂S – TiO₂ was elucidated. Mineralization of MB dye was further confirmed through Chemical Oxygen Demand measurements. The catalyst exhibited reusability. Additionally, antibacterial activity evaluation revealed that Ag₂S – TiO₂ showed potential as an effective antibacterial agent.

1. Introduction

Pollution can be influenced by different factors such as population increase, deforestation, river damming, wetland destruction, industrial activities, mining, agriculture and energy consumption. Mainly, water contamination is previously associated with population growth and industrial expansion. Wastewater incorporating chemical components like dyes, insecticides, and herbicides including biological pollutants (bacteria and viruses), was thrown into rivers and lakes by industry, and residential activities eventually ending up in the oceans. Traditionally, different treatments like flocculation, activated carbon adsorption, and filtering have been utilized for water purification. Nevertheless, these strategies are often the most costly and ineffective ones [1-3]. The advanced oxidative process

(AOP) is a unique and more efficient way of dealing with non-biodegradable contaminants [4]. The AOP uses more robust oxidants O₃, ·OH than molecular oxygen which are created by UV radiation, ultrasound, or both catalysts during the breakdown of organic contaminants [5]. In the AOP method, a semiconductor has been utilized to produce electron-hole pairs through photo-activation of the semiconductor's material. Significantly, low-energy UV light can be utilized to disintegrate refractory wastewater contaminants in the presence of a catalyst by exploiting photo-generated positive holes and electrons are potent oxidants and excellent reductants [6].

Amidst various semiconductors, nanoparticles of TiO₂ (with a bandgap energy of 3.2 eV) and ZnO (with a bandgap energy of 3.3 eV) have garnered significant



attention due to their broad potential applications, like catalysis, biology, sensing, electrical, and electronics [7]. Recently, heterogeneous semiconductors have attracted considerable interest owing to their advantageous characteristics, including low toxicity, affordability, and versatile optical, chemical, and electrical properties, as well as their ecologically friendly qualities, they are potential photocatalysts in the photocatalytic process. Nowadays, the Dopant materials can improve photocatalyst efficiency by changing the semiconductor's band gap [8], and purities [9], creating oxygen vacancies [10], and providing a unique surface area for organic molecule adsorption and electron trapper activities [11]. They can be categorized into two types: interstitial and substitutional dopants. The radius of the doped ion is smaller than that of the lattice ions or lattice spaces, allowing it to penetrate the crystal cell of the metal oxide surface in an interstitial fashion, when the dopant substitutes the lattice ion or the lattice oxide [9]. Furthermore, the doped ion in the catalyst crystal lattice has been shown to influence the electrical properties of the generated nanocatalysts enhancing its adsorption in the visible region [12-14, 9]. Because of their different shapes (spherical, cubic, hexagonal, triangle, square etc.), properties, and applications (like photocatalysis, photoluminescence, sensors, antibacterial, and more), nanoscale metal oxides and chalcogenides have been examined. Similarly, by utilizing the co-dopant compounds, the researchers hoped to improve the semiconductor properties of the material [15]. Several criteria determined the effect of doping on photocatalyst activity, including the initial concentration of pollutants, the physicochemical properties of the catalyst, and the concentration of the dopant. The photocatalytic activity decreases when the dopant concentration exceeds the appropriate doping concentration. This diminishes the catalyst's surface area narrows the space charge and boosts light penetration into the photocatalyst surface, potentially extending beyond its surface layer. Consequently, the reassembling of electron-hole pairs was more likely to occur [16-18].

It is possible to dope a semiconductor with the inclusion of transition metals, nonmetals, metals, alkaline earth metals or noble metals has been explored. Noble metals like Ag, Pt, and Au have attracted attention as doping

agents because of their ability to scavenge photogenerated electrons and enhance the separation of electron-hole pairs in the photocatalytic process. This enhances the semiconductor's photocatalytic activity [19, 20] and finally improves the organic pollutant adsorption onto the photocatalyst surface [21]. Especially Silver nanocatalysts have grown in popularity as a dopant among other noble metals due to their catalytic activity, size, shape-dependent optical properties, and promising applications in chemical and biological sensing, including surface-enhanced Raman scattering (SERS), metal fluorescence (MEF), localized surface plasmon resonance (LSPR), and antibacterial activity [22]. Furthermore, the silver is one of the most affordable noble metals. This study will concentrate on utilizing a semiconductor photocatalyst modified with silver to degrade organic pollutants (methylene blue dye). Here methylene blue dye (MB) solution serves as a model water pollutant, because of its frequent use as an essential colouring ingredient by chemical industries. Methylene blue dye is one of the most thoroughly researched organic pollutants and it is eventually discharged into water bodies through effluents and fervently recommended to remove the persistent pollutants from the aqueous solution [23-26]. The combination of TiO₂ with low band gap semiconductors like CdSe [27] and CdS [28] photocatalysts effectively removes the pollutants under visible light. The use of nanoscale coupled semiconductors to promote charge separation and minimize or prevent charge carrier recombination would considerably improve TiO₂ photocatalytic performance [29, 30]. Ag₂S is well-suited for this purpose due to its characteristics as a direct narrow-band gap semiconductor [31], offering good chemical stability and exceptional optical responses. Presently, it finds applications in optical and electronic devices like photovoltaic cells, photoconductors, infrared detectors [32, 33], and superionic conductors [34, 35]. However, there have been limited reports on the utilization of the Ag₂S-TiO₂ composite photocatalyst system for environmental purification under UV light irradiation.

2. Experimental

Materials

The commercial non-azo dye MB was purchased from Aldrich. Its chemical structure and absorption spectrum



are depicted in **Fig. 1**. Silver nitrate (99%), Sodium sulfide (99%), and titanium isopropoxide (99%) of AnalaR grade (Himedia), along with 2-propanol (99.5%

spectroscopic grade), H₂SO₄, or NaOH, were utilized as received from Sigma Aldrich. Experimental solutions were prepared using deionized water.

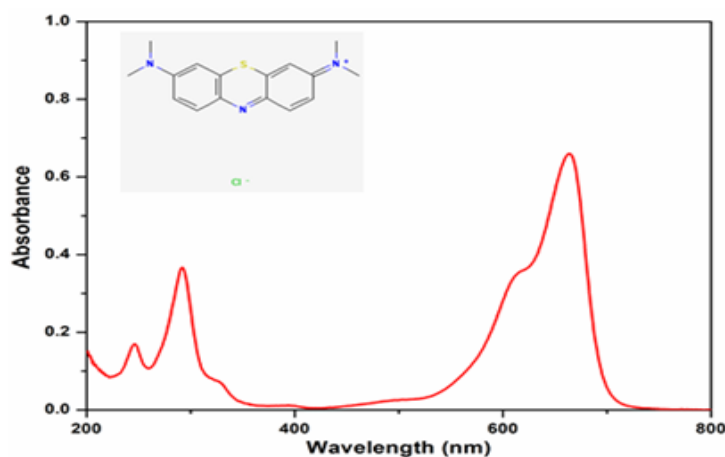


Fig. 1 The chemical structure and absorption spectrum of MB dye

Synthesis of Ag₂S-TiO₂ photocatalysts

About 0.676g of AgNO₃ was dissolved in 100 mL of distilled water (0.04 M) to prepare Solution I. Solution II was prepared by dissolving 0.184g of Na₂S in 100 mL of distilled water (0.02 M). The two solutions were mixed and stirred, resulting in the formation of an Ag₂S suspension. Subsequently, 12.5mL of titanium isopropoxide and 80mL of 2-propanol were added to the Ag₂S suspension, which was then magnetically agitated for four hours. The resulting suspension was purified, cleansed, and arid in an air oven at 100°C for 12 hours. The resulting solution was sintered in a muffle furnace for 5 hours at 450°C. The same procedure was followed to synthesize pure TiO₂.

UV-Visible Spectroscopic Analysis

The deterioration process was carried out using the Heber Multi-lamp Photoreactor HML MP 88 under UV- A light at a wavelength of 365 nm. About 50 mL of MB dye (3 X 10⁻⁴ M) containing the sufficient quantity of nanocatalysts, was agitated the dark for 30 minutes before illumination. The UV-visible spectrophotometer was employed to track variations in MB concentration based on its distinctive absorbance at 291.5 nm and the

decreased absorbance reflects the deterioration of dye occurred.

Characterization techniques

The powder X-ray diffraction pattern was analyzed using an X'Pert PRO diffractometer with Cu-K α radiation (wavelength 1.5406 Å) at a maximum power of 2.2 kW. Crystalline phases and peak positions were identified and determined through comparative analysis with standard files. The morphology of the nanocatalysts was examined using a JOEL JSM-6701F cold field emission scanning electron microscope (FE- SEM), with samples mounted on a gold substrate and inspected at various magnifications. Diffuse reflectance spectra of the synthesized nanocatalysts were examined using a Shimadzu UV-2450 diffuse reflectance spectrometer.

X-ray photoelectron spectra of the catalysts were acquired using an ESCA-3 Mark II spectrometer (VG Scientific Ltd., England) with Al K α (1486.6 eV) radiation as the source, and a calibration process was conducted to determine the binding energy of the nanocatalysts. Photoluminescence (PL) spectra were obtained using a Perkin Elmer LS 55 fluorescence spectrometer. The nanocatalyst was dispersed on a carbon tetrachloride surface and excited with light at



300 nm. UV spectra measurements for the synthesized nanocatalysts were performed using a SHIMADZU UV 2600 PC UV-visible spectrophotometer.

Chemical oxygen demand (COD) measurements

The chemical oxygen demand (COD) method was employed to determine the quantity of oxygen consumed by reactions in a given solution. The dye sample underwent reflux with HgSO_4 , a known volume of standard $\text{K}_2\text{Cr}_2\text{O}_7$, Ag_2SO_4 , and H_2SO_4 for 2 hours, followed by titration with standard Ferrous Ammonium Sulphate (FAS) using ferroin indicator. A blank titration was conducted in place of the dye samples. The COD was then calculated using the provided equation (Eq. 1).

$$\text{COD} = (\text{Blank titre value} - \text{dye sample titre value}) \times \text{normality of FAS} \times 8 \times 1000$$

$$\text{Volume of sample} \quad (1)$$

3. Results and Discussion

X-ray diffraction (XRD) spectroscopy

The crystalline size of the synthesized nanocatalysts was determined using XRD spectra as illustrated in **Fig. 2**. The X-ray diffraction peaks were located at 25.3° , 38.03° , 47.68° , 54.65° , 62.74° , 69.3° , and 75.0° corresponded to crystallographic planes (101), (004), (200), (211), (204), (220) and (215) respectively (anatase phase of TiO_2 (JCPDS 89-4203). The

crystalline anatase phase of TiO_2 has been identified to be additional active than the rutile and brookite phases [36]. The widened diffraction peaks of the synthesized nanocatalysts with Ag_2S (doped) were shifted from 25.3 to 25.7 respectively. The wideness of the peak indicates that the particle sizes of the crystalline phase were reduced [37]. However, in the instance of Ag_2S nanocatalysts, there was no indication of any diffraction peaks due to the usage of a low concentration of Ag_2S and its negligible effect on the phase of the nanocatalysts [37]. The mean crystalline size of the nanocatalysts was calculated using the classical Scherrer equation ($D = K\lambda/\beta\cos\theta$), where D represents the crystallite size, λ denotes the wavelength of the X-ray radiation ($\text{Cu- K}\alpha_1=1.54060$), K is the Scherrer constant (generally considered to be 0.9 for spherical shapes), β is the full width at half-maximum height, and θ signifies the Bragg's diffraction angle. The mean crystalline sizes of the TiO_2 and $\text{Ag}_2\text{S-TiO}_2$ nanocatalysts were found to be 34.8 nm and 11.6 nm, respectively. The average size of the $\text{Ag}_2\text{S-TiO}_2$ nanocatalysts was reduced when compared to that of the TiO_2 nanocatalysts. The difference in the particle size could be accounted for by the ionic radius of the nanocatalysts.

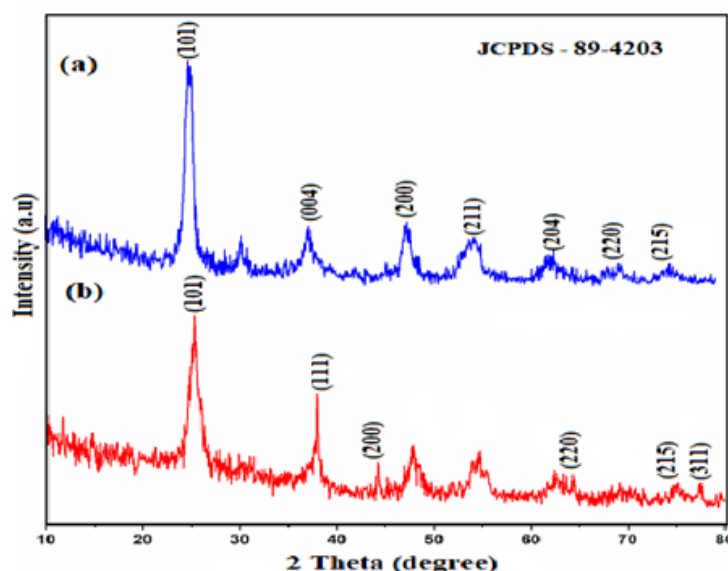
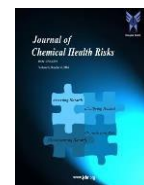


Fig. 2 Powder XRD spectrum of synthesized (a) bare TiO_2 , (b) $\text{Ag}_2\text{S-TiO}_2$ nanocatalysts



Field Emission Scanning Electron Microscopy (FE-SEM) Analysis

The superficial structure of the synthesized TiO_2 and $\text{Ag}_2\text{S-TiO}_2$ was analyzed using Field Emission Scanning Electron Microscopy (FE-SEM). The configuration and shape of the nanocatalysts were depicted in **Fig. 3 a-d** at various magnifications.

Fig. 3 a, b represented the FE-SEM images of bare TiO_2 and they show slightly aggregated and spherical

particles. The FE-SEM images of $\text{Ag}_2\text{S-TiO}_2$ **Fig. 3 c, d** can't show the aggregation. The average particle size was in the nanoscale region. The resultant particles are significantly compact with orderly arranged in the homogeneous medium, which can be attributed to the increase and densification of Ag_2S on TiO_2 .

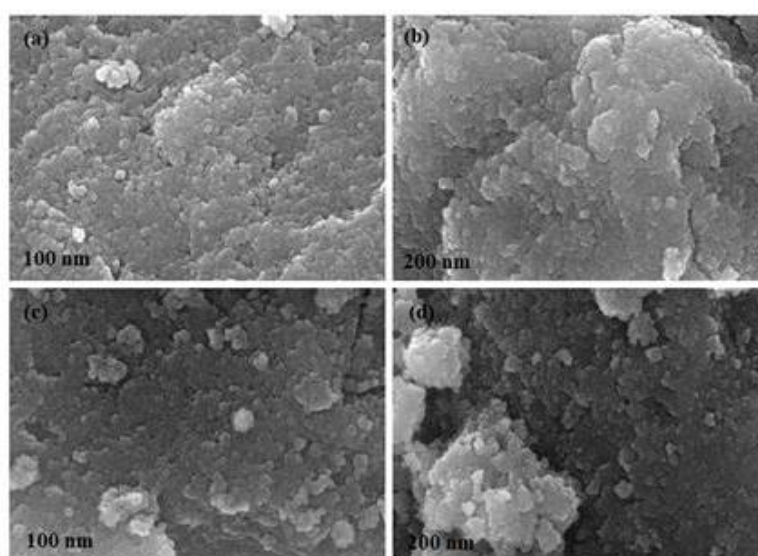


Fig. 3 FE-SEM images of (a-b) bare TiO_2 , (c-d) $\text{Ag}_2\text{S-TiO}_2$ nanocatalysts

Energy Dispersive (EDS) Spectroscopy

The Energy Dispersive Spectroscopy (EDS) of the synthesized nanocatalysts are displayed in

Fig. 4 e. The resulting EDS spectra reveal that the Ti, O, Ag and S elements are presented in the synthesized nanocatalysts.

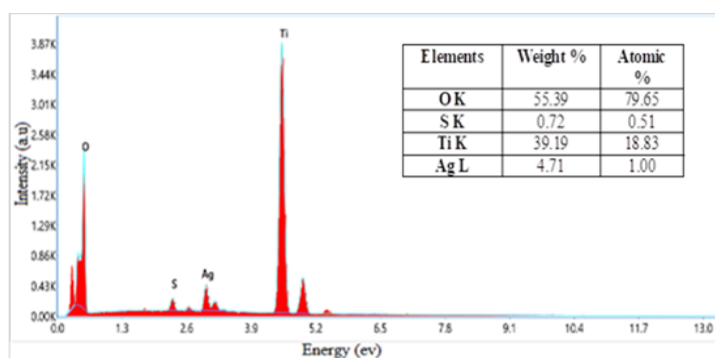


Fig. 4 EDS spectrum of $\text{Ag}_2\text{S-TiO}_2$ nanocatalysts



UV-DRS spectroscopy

The diffuse reflectance spectra of prepared TiO₂ and Ag₂S-TiO₂ are shown in **Fig. 5 a, b**. Ag₂S-TiO₂ exhibits higher absorption than bare TiO₂ in both UV and Visible regions, potentially enhancing the catalyst's activity.

The UV-visible spectra, recorded in diffuse reflectance mode (R), were converted into the Kubelka-Munk function F(R) to differentiate the extent of light absorption from scattering.

$$(F(R)E)^{1/2} = \frac{[(1-R)^2 \times h\nu]^{1/2}}{2R} \quad (2)$$

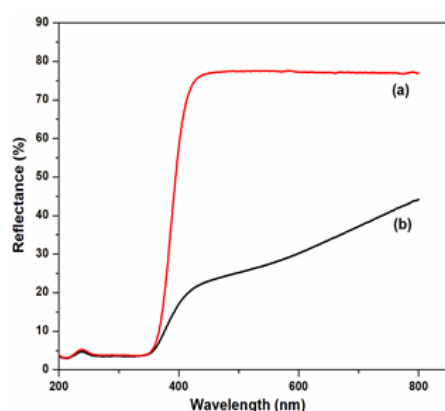


Fig. 5 DRS of (a) bare TiO₂ and (b) Ag₂S-TiO₂ nanocatalysts

Photoluminescence (PL) Spectroscopy

The capability of charge carrier entrapment, migration, and shift, in addition to the rapid electron-hole (e⁻-h⁺) couplings in semiconductor nanocatalysts, were investigated by photoluminescence spectroscopy (PL). **Fig. 7 a, b** depicts the PL emission spectra of bare TiO₂ and Ag₂S-TiO₂ nanocatalysts. The

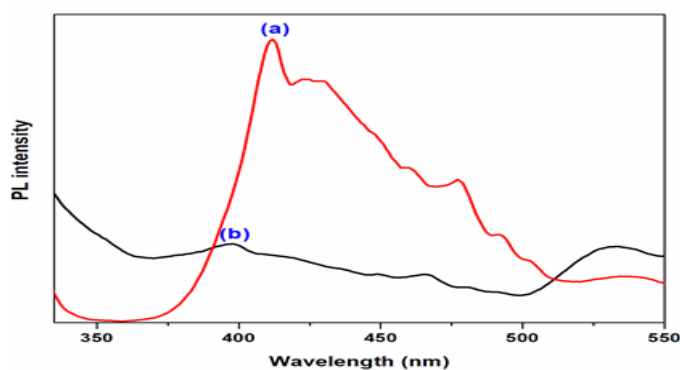


Fig. 7 photoluminescence spectra of (a) bare TiO₂ and (b) Ag₂S-TiO₂ nanocatalysts

The bandgap energy (E_g) of each sample was calculated from the intersection of a straightway derived from the graph of the K-M function versus the absorbed photon energy (E) (Eq. 2). The obtained band gap energy values are 3.15 eV and 2.95 eV for the bare TiO₂ and Ag₂S-TiO₂ nanocatalysts, respectively **Fig. 6 a, b**. Ag₂S-TiO₂ absorbs more ultraviolet and visible light than bare TiO₂, which may boost the activity of the nanocatalysts.

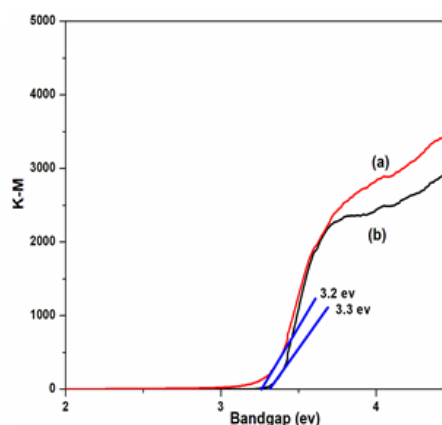


Fig. 6 bandgap energy of (a) bare TiO₂ and (b) Ag₂S-TiO₂ nanocatalysts

photoluminescence was caused by the reassembling of electron-hole pairs in semiconductor nanocatalysts. The investigated PL spectra of bare TiO₂ have greater intensity than the Ag₂S-TiO₂ nanocatalysts. The lower emission intensity of the Ag₂S-TiO₂ indicates that Ag₂S particles effectively limit charge carrier recombination, which would increase photocatalytic activity.



X-ray Photo Electron (XPS) Spectroscopy

X-ray Photo Electron Spectroscopy detects the chemical states and types of bonds between the nanocatalysts of TiO_2 and $\text{Ag}_2\text{S-TiO}_2$. The survey X-ray photoelectron spectra of TiO_2 and $\text{Ag}_2\text{S-TiO}_2$ nanocatalysts are given in **Fig. 8 a.** and **Fig. 8 b** shows the Spin-Orbit components ($2p_{3/2}$ and $2p_{1/2}$) of the Ti 2p peaks at 458.3 and 464.0 eV, thus indicating the presence of Ti^{4+} [38]. The presence of

oxygen species is demonstrated by the appearance of O 1s peak at 529.69 eV in **Fig. 8 c** [39].

The resulting Ag $3d_{5/2}$, and Ag $3d_{3/2}$ peaks are attributed at 367.5 eV and 373.61 eV in **Fig. 8 d** respectively. In this spectra, there is no splitting of Ag $3d_{5/2}$ and Ag $3d_{3/2}$ peaks, indicating that Ag in $\text{Ag}_2\text{S-TiO}_2$ exists solely as an Ag^+ ion [40]. Sulphur $2p_{3/2}$ occurred at 168.08 eV **Fig. 8 e** [41].

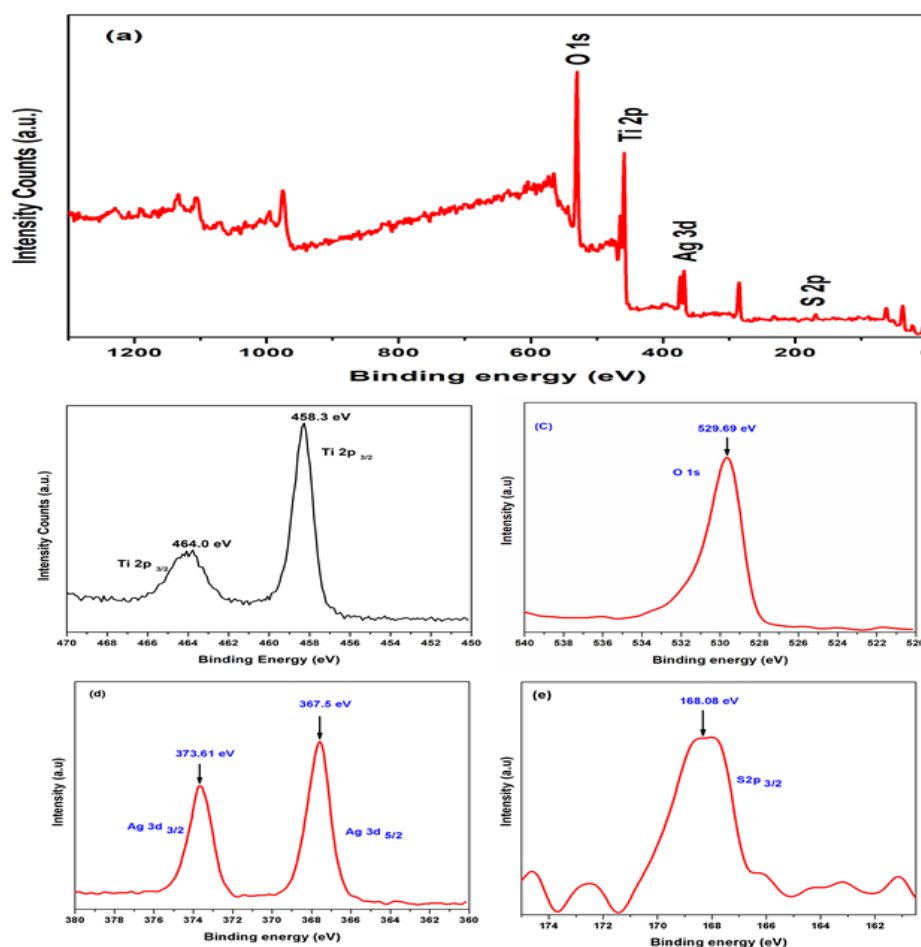


Fig. 8 XPS of $\text{Ag}_2\text{S-TiO}_2$ nanocatalysts: (a) survey spectrum, (b) Ti2p peak, (c) O1s peak, (d) Ag 3d peak and (e) S 2p peak.

Photocatalytic Activity Investigations

Fig. 9 shows the remaining amount of MB dye (3×10^{-4} M) after UV light irradiation both in the absence and presence of various photocatalysts. The result shows that the utilized $\text{Ag}_2\text{S-TiO}_2$ nanocatalysts for 40 minutes

of UV radiation which provides the 90.3% deterioration efficiency of the MB dye (curve f), significantly. Curve b represents the 55.3% decreased concentration of the MB dye with the same technique without UV light irradiation due to the catalyst adsorbed on the dye



molecule. The resulting blank reaction was permitted to proceed in the existence of UV irradiation and a negligible concentration (0.5%) was measured (curve a). These results indicated the successful deterioration efficiency of MB dye by using UV-A light irradiation and the significant photocatalytic activity of the $\text{Ag}_2\text{S-TiO}_2$ nanocatalysts. Under the same conditions for the

commercial ZnO , TiO_2 and Ag_2S deterioration rates are 50% (curve d), 63.8% (curve e), and 25.9% (curve c), respectively **Fig. 9**. This reveals that the UV/ $\text{Ag}_2\text{S-TiO}_2$ technique degrades the MB dye in more effectively than the other procedures. The effect of operational parameters was explored to determine the optimal circumstances utilized by the $\text{Ag}_2\text{S-TiO}_2$ nanocatalysts.

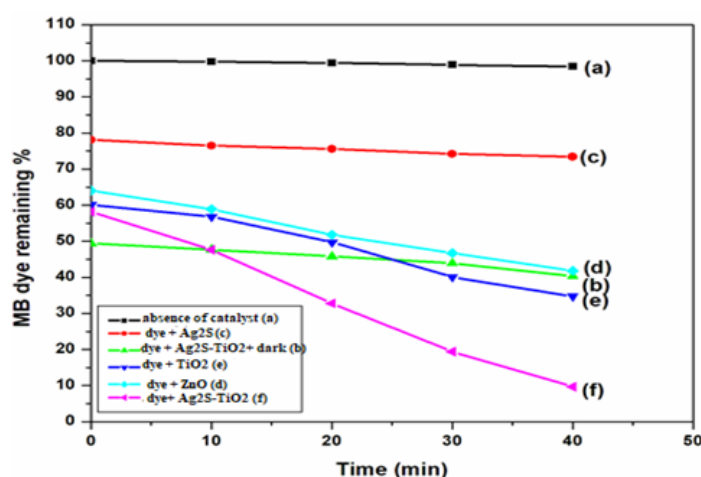


Fig. 9 Photodegradability of MB dye using UV $\text{Ag}_2\text{S-TiO}_2$ nanocatalysts:

$[\text{MB}] = 3 \times 10^{-4} \text{ mol/L}$, $\text{pH} = 7.0 \pm 0.1$, $\text{Ag}_2\text{S-TiO}_2$ nanocatalysts = 2 g/L ,

$I_{\text{UV}} = 1.381 \times 10^{-6} \text{ Einstein L}^{-1} \text{ s}^{-1}$, airflow rate = 8.1 mL s^{-1} , time = 40 min.

Fig. 10 illustrates the UV-visible spectra of the solution of MB dye ($3 \times 10^{-4} \text{ M}$) at various irradiation time intervals. The displayed UV-Vis spectra of the $\text{Ag}_2\text{S-TiO}_2$ nanocatalysts do not show any significant variation during the irradiation and the intensity of the

dye diminished gradually with deterioration at 291.5 nm and 663.5 nm respectively. This diminished intensity indicates that these intermediates do not absorb any light irradiation.

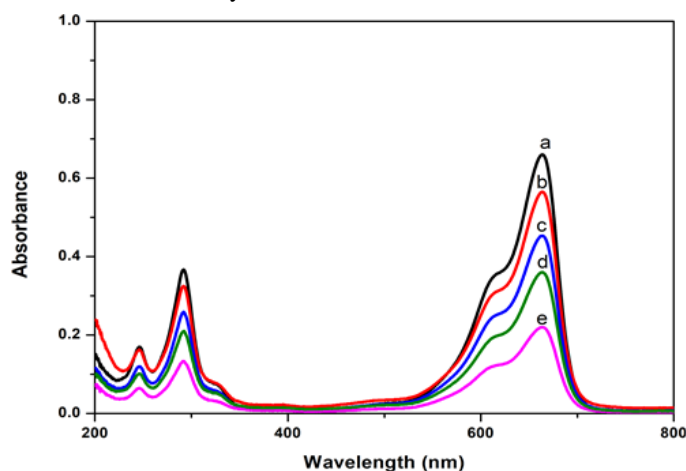


Fig. 10 The changes in UV-visible spectra of MB on irradiation with UV light in the presence of $\text{Ag}_2\text{S-TiO}_2$ nanocatalysts: $[\text{MB}] = 3 \times 10^{-4} \text{ mol/L}$, $\text{pH} = 7.0 \pm 0.1$, $\text{Ag}_2\text{S-TiO}_2$ nanocatalysts = 2 g/L , a) 0 min, b) 10 min, c)



20 min, d) 30 min, e) 40 min, $I_{UV} = 1.381 \times 10^{-6}$ Einstein $L^{-1} s^{-1}$, airflow rate = 8.1 mL s^{-1} .

Influence of the operational parameters

Impact of pH

The pH of the solution played a crucial role in the photocatalytic deterioration techniques of abundant pollutants [42, 43]. The photocatalytic deterioration process of the MB dye was influenced by different pH levels ranging from 3-11. Before irradiation, the pH was adjusted and couldn't be monitored during the reaction. Furthermore, the various pH levels of the MB dye were influenced by the surface charge characteristics of TiO_2 ,

molecular charge, chemisorption of dye molecules onto the Ag_2S-TiO_2 surface and hydroxyl radical concentration. The deterioration of the MB dye as a function of irradiation time and pH was depicted in **Fig. 11**. According to the findings, the photocatalytic deterioration capability of Ag_2S-TiO_2 was greater at neutral pH 7. The adsorption percentages at different pH levels (3, 5, 7, 9 and 11) were provided to 30.9, 42.1, 55.3, 42.3, and 25.1%, respectively. Significantly, the increased deterioration efficiency at pH 7 was owing to the higher absorbance of MB dye on the superficial catalyst.

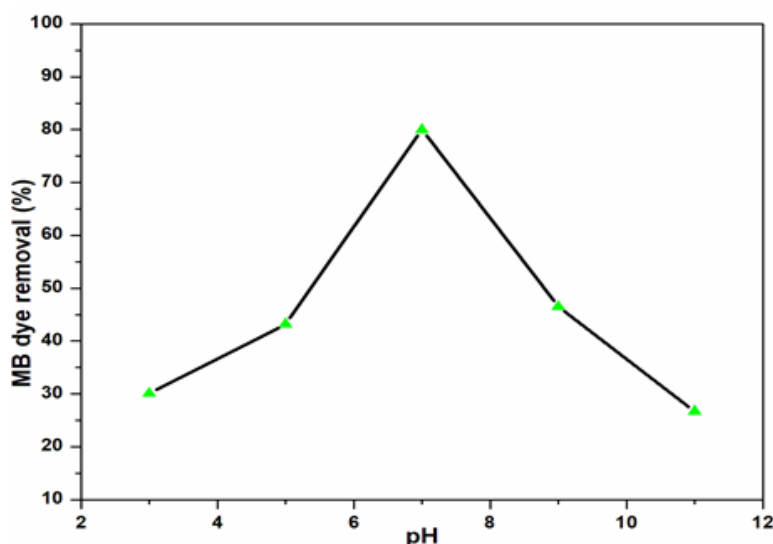


Fig. 11 Effect of initial pH on the degradation of MB using UV light/ Ag_2S-TiO_2 nanocatalysts: $[MB] = 3 \times 10^{-4} \text{ mol/L}$, Ag_2S-TiO_2 nanocatalysts = 2 g/L , $I_{UV} = 1.381 \times 10^{-6}$ Einstein $L^{-1} s^{-1}$, airflow rate = 8.1 mL s^{-1} , time = 30 min.

Impact of the catalyst

The dosage of catalyst was one of the most important criteria in deterioration research. To prevent excessive use of the catalyst, it is essential to determine the removal of dye molecules [44–47]. The photocatalytic deterioration rate was investigated using various catalyst concentrations, scale from 0.5 to 3 g/L. The outcomes are displayed in **Fig. 12**, as the catalyst concentration increases from 0.5 to 2 g/L at 30 minutes of irradiation and the deterioration percentages can be

increased from 12.6 to 80.0% respectively. As a result, the quantity of Ag_2S-TiO_2 nanocatalysts has grown, which boosts photon absorption and dye adsorption. If the amount of Ag_2S-TiO_2 nanocatalysts is increased (over 2 g/L), the rate of elimination decreases due to the presence of the screening effect [48]. Finally, the determined quantity of nanocatalysts loaded for the MB dye deterioration was found to be 2 g/L, and it is the suitable amount of catalyst for effective deterioration.

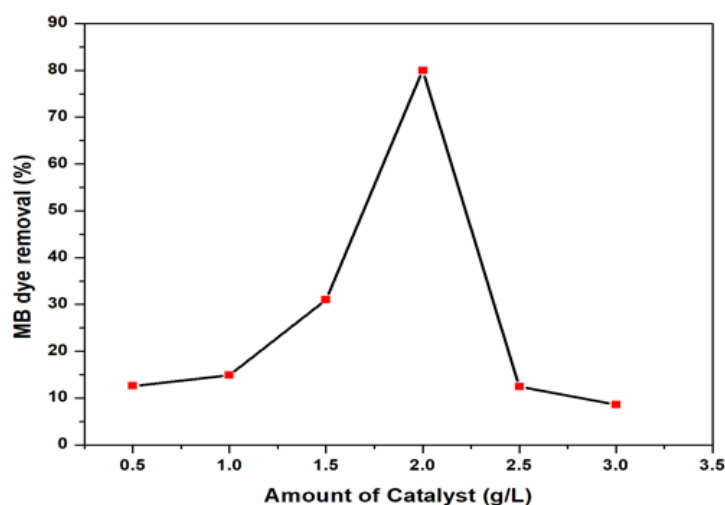


Fig. 12 Effect of catalyst weight on the photocatalytic degradation of MB using UV light: [MB] = 3×10^{-4} mol/L, pH = 7.0 ± 0.1 , $I_{UV} = 1.381 \times 10^{-6}$ Einstein $L^{-1} s^{-1}$, airflow rate = 8.1 mL s^{-1} , time = 30 min.

Impact of starting dye concentration

The effects of different concentrations of MB dye deterioration are illustrated in Fig. 13. The results revealed that increasing the dye concentration from 1 to 5×10^{-4} M resulted in a reduction in deterioration from 93.8 to 41.2% at 30 minutes. The rate of deterioration was directly proportional to the amount of $\cdot\text{OH}$ on the catalyst surface, along with the interaction of $\cdot\text{OH}$ radicals with the dye molecule. Throughout all starting dye concentrations, the catalyst amount and light

intensity remain constant. As the initial dye concentration increased, the path length of the photons entering increased, leading to a diminished photocatalytic deterioration capability at low concentrations; conversely, increasing the concentration boosted photon capture by the catalyst [43]. The substantial dosage of dye accumulated may compete with oxygen and OH adsorption on the superficial catalyst.

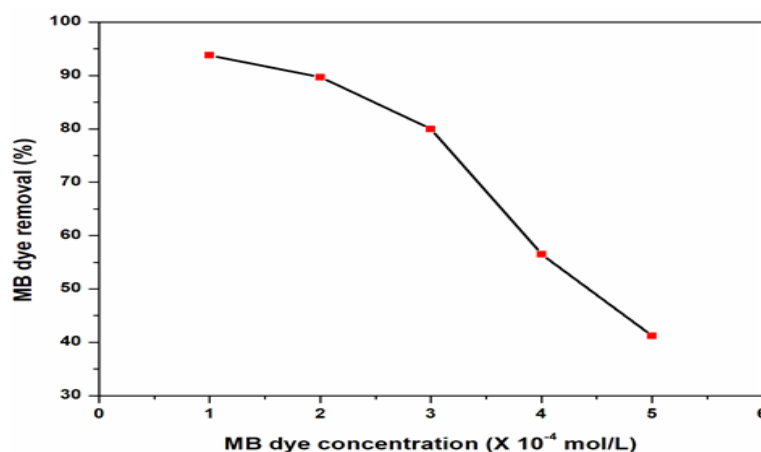


Fig. 13 Effect of various initial dye concentrations on the degradation of MB using UV light/ $\text{Ag}_2\text{S-TiO}_2$ nanocatalysts: pH = 7.0 ± 0.1 , $\text{Ag}_2\text{S-TiO}_2$ nanocatalyst = 2 g/L, $I_{UV} = 1.381 \times 10^{-6}$ Einstein $L^{-1} s^{-1}$, airflow rate = 8.1 mL s^{-1} , time = 30 min.

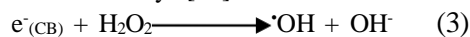


Effect of oxidants

Impact of H₂O₂

The effect of adding H₂O₂ upon the photocatalytic oxidation has been displayed in **Fig. 14**. About 10 mmol of H₂O₂ can boost the deterioration rate from 80 to 92.7% in 30 minutes. H₂O₂ can capture the photogenerated conduction band electron, preventing electron-hole recombination and generating hydroxyl radicals (Eq. 3). Hydroxyl radicals play a crucial role in the deterioration of pollutants [49]. However, the removal rate decreases with high H₂O₂ dosage (beyond 10 mmol) due to the hydroxyl radical scavenging effect

of H₂O₂. Excess hydrogen peroxide reacts with the hydroxyl radical ([•]OH) to produce hydroperoxy radical ([•]HO) (Eq. 4, 5). These hydroperoxy radicals were significantly less reactive and do not contribute to the oxidation of the dye [50].



At higher dosage,

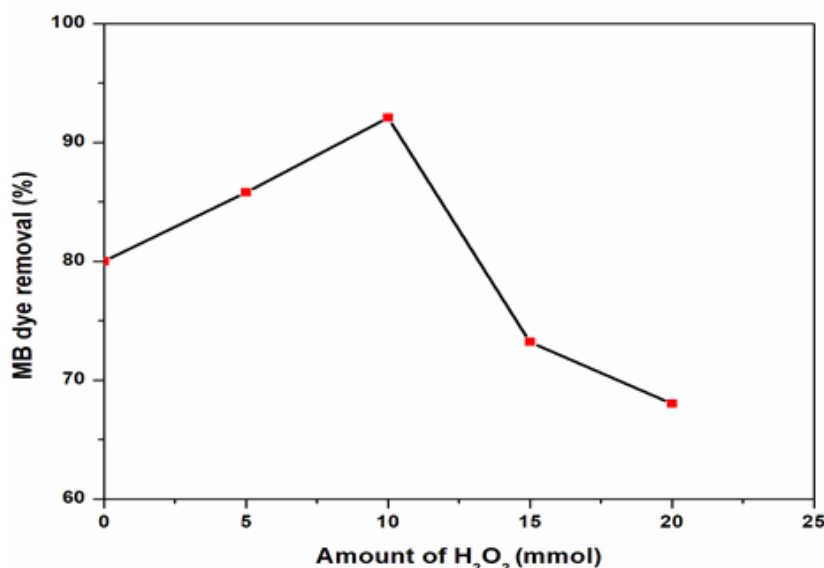
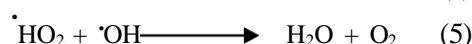


Fig. 14 Effect of H₂O₂ on the degradation of MB using UV light/Ag₂S-TiO₂ nanocatalysts: pH = 7.0±0.1, Ag₂S-TiO₂ nanocatalysts = 2g/L, I_{UV} = 1.381×10⁻⁶ Einstein L⁻¹ s⁻¹, airflow rate = 8.1 mL s⁻¹, time = 30 min.

Impact of K₂S₂O₈

The photocatalytic deterioration of the MB dye was examined by increasing the dosage of K₂S₂O₈ from 5 to 20 mg/50 mL and displayed in **Fig. 15**. The addition of K₂S₂O₈ up to 15 mg accelerates deterioration from 80 to 90.3% after 30 minutes and further, addition (above 15 mg) reduces the deterioration [51, 52]. The sulfate radical anion can combine with both the photogenerated electrons and water molecules to produce hydroxyl radicals (Eq. 6-8).

The sulfate radical anion (SO₄^{•-}) played an important role in the deterioration methods. At large doses of S₂O₈²⁻ to inhibit the deterioration rate due to the

increasing concentration of SO₄²⁻ ions. The extra SO₄²⁻ ions are adsorbed upon the TiO₂ surface to reduce the catalytic activity.



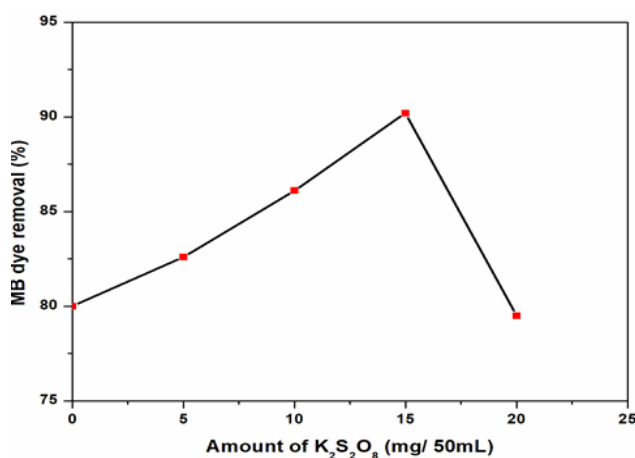


Fig. 15 Effect of $K_2S_2O_8$ on the degradation of MB using UV light/ Ag_2S-TiO_2 nanocatalysts: pH = 7.0 ± 0.1 , Ag_2S-TiO_2 nanocatalysts = 2g/L, $I_{UV} = 1.381 \times 10^{-6}$ Einstein $L^{-1} s^{-1}$, airflow rate = 8.1 $mL s^{-1}$, time = 30 min.

Impact of Na_2CO_3

Fig. 16 shows the effect of Na_2CO_3 on the photocatalytic deterioration for MB. This study demonstrated that increasing the addition of Na_2CO_3 reduces the removal efficiency. The result shows the addition of Na_2CO_3 (upto 20 mg) reduces the

removal rate from 80 to 33.7% after 30 minutes [53]. The carbonate ion concentration can be increased, and the hydroxyl radical gradually diminishes and significantly reduces the photocatalytic deterioration (Eq. 9).

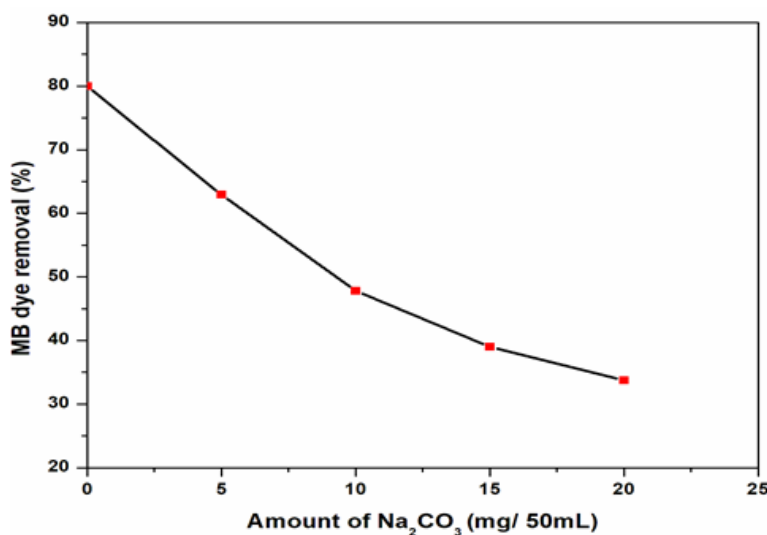


Fig. 16 Effect of Na_2CO_3 on the degradation of MB using UV light/ Ag_2S-TiO_2 nanocatalysts: pH = 7.0 ± 0.1 , Ag_2S-TiO_2 nanocatalysts = 2g/L, $I_{UV} = 1.381 \times 10^{-6}$ Einstein $L^{-1} s^{-1}$, airflow rate = 8.1 $mL s^{-1}$, time = 30 min.



Impact of NaCl

The MB deterioration was investigated using NaCl and displayed in **Fig. 17**. Additionally, the Cl^- ions up to 20 mg to the reaction solution resulted in a deterioration rate falling from 80 to 37.2% after 30 minutes. The decrease in the deterioration efficiency

was attributed to the hole scavenging characteristics of chloride ions (Eq. 10), and the dye molecule with the hole competes with these reactions [54].

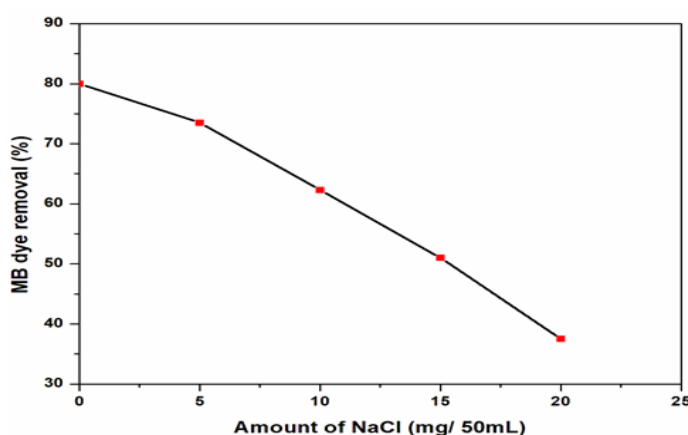


Fig. 17 Effect of NaCl on the degradation of MB using UV light/ $\text{Ag}_2\text{S-TiO}_2$ nanocatalysts: $\text{pH} = 7.0 \pm 0.1$, $\text{Ag}_2\text{S-TiO}_2$ nanocatalysts = 2g/L, $I_{\text{UV}} = 1.381 \times 10^{-6} \text{ Einstein L}^{-1} \text{ s}^{-1}$, airflow rate = 8.1 mL s^{-1} , time = 30 min.

Catalyst reusability

Significantly catalyst reusability is crucial to reduce the overall cost of the process. The determined deterioration efficiencies of the dye were discovered in **Fig. 18**. The resulting deterioration of dye at the first, second, third, fourth, and fifth runs were indexed at

90.3, 83.5, 76.2, 68, and 60%, respectively. These results indicate that the $\text{Ag}_2\text{S-TiO}_2$ nanocatalysts had excellent photostability and reusability, with no appreciable decline in photocatalytic activity over five runs in the presence of UV-A light.

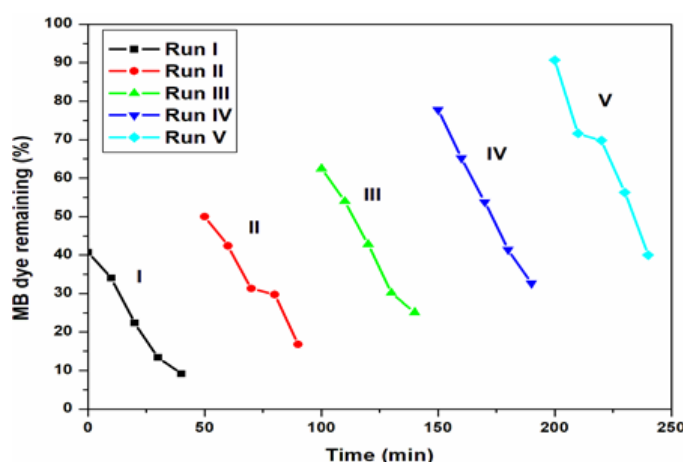


Fig. 18 Catalyst reusability: $\text{MB} = 3 \times 10^{-4} \text{ mol/L}$, $\text{pH} = 7.0 \pm 0.1$, $\text{Ag}_2\text{S-TiO}_2$ nanocatalysts = 2g/L, $I_{\text{UV}} = 1.381 \times 10^{-6} \text{ Einstein L}^{-1} \text{ s}^{-1}$, airflow rate = 8.1 mL s^{-1}



Radical Scavengers Test

The impact of various radical scavengers such as 2-propanol, ethylenediamine tetraacetic acid, and benzoquinone on photocatalytic deterioration was analyzed and displayed in Table 1. In the absence of scavengers, photocatalytic deterioration proceeded at an accelerated rate (90.3%), as illustrated in Table 1. When 2-propanol was added, deterioration was reduced (67.2%) due to the scavenger's ability to eliminate hydroxyl radicals ($\cdot\text{OH}$), thereby reducing the deterioration rate. Ethylenediamine tetraacetic acid and

benzoquinone were used to remove h^+ and $\text{O}_2^{\cdot-}$ radical anions, respectively. Additionally, benzoquinone and ethylenediamine tetraacetic acid diminished deterioration, resulting in rates of 55.4% and 43.1%, respectively. All scavengers decreased the deterioration capability of the catalyst, with the inclusion of EDTA crucially reducing the deterioration capability, indicating that holes (h^+), radicals ($\cdot\text{OH}$), and radical anions ($\text{O}_2^{\cdot-}$) were active species in the deterioration mechanisms.

Table 1 Effects of different radical scavengers on the photodegradation of MB dye under UV radiation utilizing $\text{Ag}_2\text{O-TiO}_2$ nanocatalysts

Different radical scavengers	MB dye degradation percentage (%)
No scavenger	90.3
2-propanol	67.2
Benzoquinone	55.4
Ethylenediaminetetraacetic acid	43.1

Kinetic analysis

The deterioration of MB dye under photocatalysis followed pseudo-first-order kinetics when using the $\text{Ag}_2\text{S-TiO}_2$ nanocatalysts. The provided equation presented the rate expression applicable. The provided equation presented the rate expression applicable for low starting concentrations of the substrate (MB) dye

$$-\frac{d[\text{C}]}{dt} = k'[\text{C}] \quad (11)$$

Where k represented the rate constant of pseudo-first order. The deterioration rate constant is detailed in Table 2.

Table 2 Rate constants of photocatalytic deterioration of MB dye using UV light/ $\text{Ag}_2\text{S-TiO}_2$ nanocatalysts

Initial concentration of dye X (10^{-4}) mol/L	Degradation
1	0.0627
2	0.0517
3	0.0453
4	0.0339
5	0.0259

Adsorption-desorption equilibrium was attained as MB dye accumulated onto the surface of the $\text{Ag}_2\text{S-TiO}_2$ nanocatalysts. The equilibrium concentration of MB dye was determined from the adsorption process and utilized as the starting point for kinetic analysis. By integrating the preceding equation under the limit of $C = C_0$ at $t = 0$,

$$\ln \frac{[C_0]}{[C]} = k't \quad (12)$$

Where C_0 represented the equilibrium concentration of the bulk solution, C_0 denoted the equilibrium concentration of MB, and C signified the current concentration. The obtained rate constant of $\ln(C_0/C)$ was plotted against the deterioration time as shown in Fig. 19. A linear relationship was observed between MB dye concentration and irradiation time.



The Langmuir-Hinshelwood (L-H) kinetic expression, widely utilized in heterogeneous photocatalytic processes [54, 55], was modified to account for the solid-liquid reaction [56], aligning with the experimental results.

The rate of MB oxidation was determined by the adsorption of MB on $\text{Ag}_2\text{S-TiO}_2$ [57].

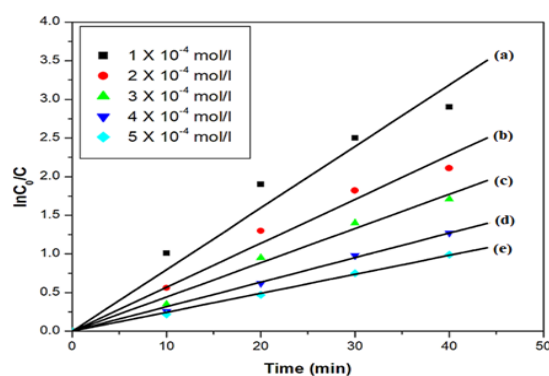


Fig. 19 Kinetics of MB dye degradation for different initial concentration by UV light/ $\text{Ag}_2\text{S-TiO}_2$ nanocatalysts: $\text{pH} = 7.0 \pm 0.1$, $\text{Ag}_2\text{S-TiO}_2$ nanocatalysts = 2g/L, $I_{\text{UV}} = 1.381 \times 10^{-6} \text{ Einstein L}^{-1} \text{ s}^{-1}$, airflow rate = 8.1 mL s^{-1} .

The impact of dye concentration on the rate of deterioration was described by the following equations (Eq. 13, 14).

$$r = \frac{K_1 K_2 C}{1 + K_1 C} \quad (13)$$

$$\frac{1}{r} = \frac{1}{K_2 K_1 C} + \frac{1}{k_2} \quad (14)$$

Where 'C' represented the MB concentration at time 't', K_1 was indicated as the adsorption constant, and K_2 was associated with the reaction characteristics of the substrate (MB). **Fig. 20** represented the linear plot attained by graphing the reciprocal of the initial rate ($1/r$) versus the reciprocal of the initial concentration of MB ($1/C$), indicating that the application of the L-H equation significantly aided in the dye deterioration. K_1 and K_2 were determined from the slope, intercept were $5.96 \times 10^3 \text{ M}^{-1}$ and $1.84 \times 10^{-5} \text{ Mm}^{-1}$ respectively.

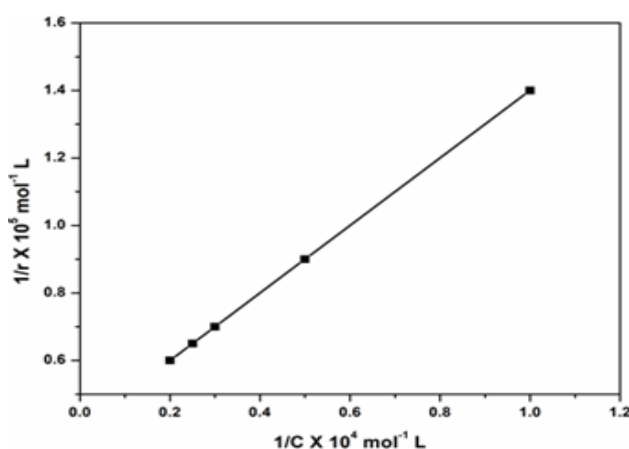


Fig. 20 Linearized reciprocal kinetic plot of the degradation of MB by $\text{Ag}_2\text{S-TiO}_2$ nanocatalysts

Chemical Oxygen Demand (COD) analysis

The COD results were used to confirm the MB dye mineralization and the decreased value of COD % was shown in **Table 3**. The results demonstrated a significant decrease in COD values in the solutions

obtained after photodegradation. This indicates that 86.4% of COD removal was obtained for MB dye deterioration within 40 minutes. It proves the mineralization of dye.

Table 3 COD values and removal rate by UV/ $\text{Ag}_2\text{S-TiO}_2$ nanocatalysts

Time (min)	COD Values (mg/L)	COD removal (%)
0	8780.8	0
20	5376	38.8
40	1164.8	86.4

Mechanism of deterioration

Fig. 21 displayed the excitation, and charge transfer mechanism between Ag_2S and TiO_2 nanocatalysts under visible light illumination. Electrons and holes were generated when $\text{Ag}_2\text{S-TiO}_2$ nanocatalysts was revealed to UV-A light irradiation. Electrons moved from the Conduction Band of Ag_2S to the Conduction Band of TiO_2 , whilst holes migrated from the Valence Band of TiO_2 to the Valence Band of Ag_2S . This electron transfer process occurred at rapidly compared to electron-hole recombination. The resulting holes reacted with surface adsorbed water or hydroxyl ions, producing the strong oxidant hydroxyl

radical ($\cdot\text{OH}$). Conversely, electrons were scavenged by oxygen molecules, generating the highly reactive superoxide radical anion ($\text{O}_2^{\cdot-}$). Ultimately, both radicals exhibited high reactivity, contributing to the deterioration of dye molecules.



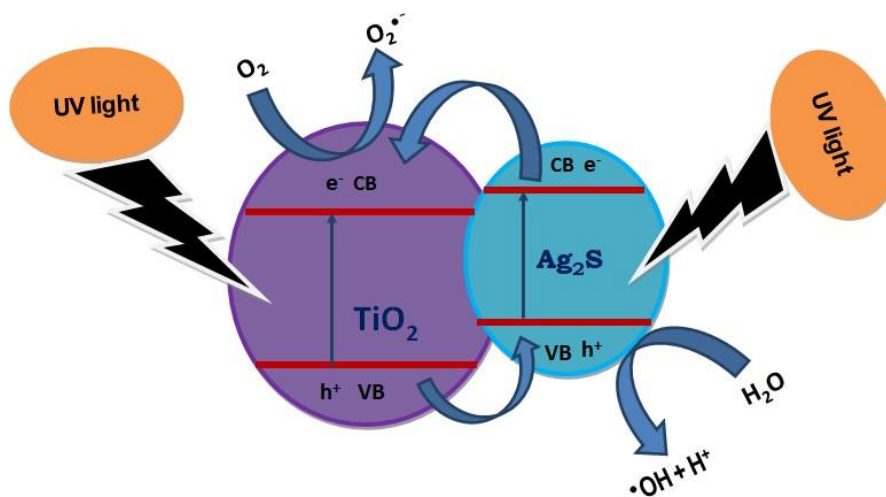


Fig. 21 Mechanism of dye deterioration

Antibacterial studies

Antimicrobial activity was assessed using the well diffusion techniques. Gram-positive bacteria such as *Staphylococcus aureus* and *Micrococcus lutes*, along with Gram-negative bacteria like *E. coli* and *Salmonella typhi*, were included in the test. The control consisted of filter paper without any nanocatalysts, while the standard treatment involved Chloramphenicol administration. Test pathogens were cultured on Muller Hinton Agar plates for antibacterial evaluation. Wells were formed using a sterile cork borer, loaded with the appropriate doses of nanocatalysts (Ag_2S , $\text{Ag}_2\text{S-TiO}_2$, TiO_2), and then placed

upon the agar. The plates were incubated for 24 hours at 37°C . Activity against the test pathogens was assessed by measuring the diameter of the inhibition zone (mm). One well contained the standard (Chloramphenicol), while three other wells held various nanocatalysts (Ag_2S , $\text{Ag}_2\text{S-TiO}_2$, TiO_2). The results were tabulated in Table 4. Ag_2S and TiO_2 alone exhibited inadequate activity against all tested bacterial strains. Conversely, the $\text{Ag}_2\text{S-TiO}_2$ nanocatalysts demonstrated superior antibacterial activity compared to Ag_2S and TiO_2 individually **Table 4**. Remarkably, $\text{Ag}_2\text{S-TiO}_2$ exhibited enhanced activity against *Micrococcus lutes* compared to other microorganisms.

Table 4 Antimicrobial activity of Ag_2S , $\text{Ag}_2\text{S-TiO}_2$, TiO_2 and Standard (Chloramphenicol)

S. No	Microorganisms	Zone of inhibition (mm) 50($\mu\text{g/ml}$)			
		Ag_2S	$\text{Ag}_2\text{S-TiO}_2$	TiO_2	Standard (Chloramphenicol)
Gram positive bacteria					
1	<i>Staphylococcus aureus</i>	15	18	16	25
2	<i>Micrococcus lutes</i>	17	19	14	24
Gram negative bacteria					
3	<i>E.coli</i>	15	17	13	24
4	<i>Salmonella typhi</i>	16	18	15	22



Conclusion

The precipitation-thermal decomposition process was utilized to synthesize Ag₂S loaded TiO₂ nanocatalysts. The loading of Ag₂S on TiO₂ was analysed using several analytical methods like XRD, FE-SEM, EDS, UV-DRS, PL, and XPS. The

visible light absorption of Ag₂S-TiO₂ nanocatalysts is more than pure TiO₂. PL spectra indicated that the presence of the presence of Ag₂S loaded on TiO₂ suppresses the recombination of photogenerated electron-hole pairs. XPS analysis confirmed the existence of Ti, O, Ag, and S components. Essentially, the Ag₂S-TiO₂ nanocatalysts exhibited higher efficiency than bare TiO₂ under UV light illumination, making it more suitable for wastewater treatment.

Acknowledgement

Authors are thankful to Prof. Dr. M. Swaminathan, Emeritus professor (CSIR), Nanomaterial laboratory, Department of Chemistry, Kalasalingam Academy of Research and Education, Krishnankoil, Tamil Nadu for his valuable suggestions and help.

4. References

- [1] Mohamed EF (2011) 'Removal of organic compounds from water by adsorption and photocatalytic oxidation', Doctoral dissertation, University of Toulouse.
- [2] Oturan MA, Aaron JJ (2014) Advanced oxidation processes in water/wastewater treatment: principles and applications. A review. *Critical Reviews in Environmental Science and Technology*, 44, 2577-2641.
- [3] Krishnan S, Rawindran H, Sinnathambi C, Lim J (2017) Comparison of various advanced oxidation processes used in remediation of industrial wastewater laden with recalcitrant pollutants. *Materials Science and Engineering*, 206(1) 12-86.
- [4] Gnanaprakasam A, Sivakumar V, Thirumarimurugan M (2016) A study on Cu and Ag doped ZnO nanoparticles for the photocatalytic degradation of brilliant green dye: synthesis and characterization. *Water Science and Technology*, 74, 1426-1435.
- [5] Vora J, Chauhan S, Parmar K, Vasava S, Sharma S, Bhutadiya L (2009). Kinetic study of application of ZnO as a photocatalyst in heterogeneous medium. *Journal of Chemistry*, 6, 531- 536.
- [6] Bamuza-pemu EE (2014) 'Photocatalytic degradation of phenolic compounds and algal metabolites in water'. Doctoral dissertation, University of Pretoria.
- [7] Ibhaddon AO, Fitzpatrick P (2013) Heterogeneous photocatalysis: recent advances and applications. *Catalysts*, 3, 189-218.
- [8] Sathishkumar P, Mangalaraja RV, Anandan S, Ashokkumar M (2013) CoFe₂O₄/TiO₂ nanocatalysts for the photocatalytic degradation of Reactive Red 120 in aqueous solutions in the presence and absence of electron acceptors. *Chemical engineering journal*, 220, 302-310.
- [9] Cao Y, Yu Y, Zhang P, Zhang L, He T, Cao Y (2013) An enhanced visible-light photocatalytic activity of TiO₂ by nitrogen and nickel-chlorine modification. *Separation and Purification Technology*, 104, 256-262.
- [10] Wu M, Yang B, Lv, Y, Fu Z, Xu J, Guo T, Zhao Y (2010) Efficient one-pot synthesis of Ag nanoparticles loaded on N-doped multiphase TiO₂ hollow nanorod arrays with enhanced photocatalytic activity. *Applied Surface Science*, 256, 7125-7130.
- [11] Barakat M, Al-hutailah R, Qayyum E, Rashid J, Kuhn J (2014) Pt nanoparticles/TiO₂ for Photocatalytic degradation of phenols in wastewater.



- Environmental technology, 35, 137.
- [12] Tian B, Zhang J, Tong T, Chen F (2008) Preparation of Au/TiO₂ catalysts from Au(I)-thiosulfate complex and study of their photocatalytic activity for the degradation of methyl orange. *Applied Catalysis B: Environmental*, 79, 394-401.
- [13] Pouretdal HR, Eskandari H, Keshavarz MH, Semnani A (2009a) Photodegradation of Organic Dyes using Nanoparticles of Cadmium Sulfide Doped with Manganese, Nickel and Copper as Nanophotocatalyst. *Acta Chimica Slovenica*, 56.
- [14] Tian B, Li C, Gu F, Jiang H, Hu Y, Zhang J (2009) Flame sprayed V-doped TiO₂ nanoparticles with enhanced photocatalytic activity under visible light irradiation. *Chemical Engineering Journal*, 151, 220-227.
- [15] Boxi SS, Paria S (2014) Effect of silver doping on TiO₂, CdS, and ZnS nanoparticles for the photocatalytic degradation of metronidazole under visible light. *RSC Advances*, 4, 37752-
- [16] XU AW, GAO Y, LIU HQ (2002) The preparation, characterization, and their photocatalytic activities of rare-earth-doped TiO₂ nanoparticles. *Journal of Catalysis*, 207, 151-
- [17] Gnanaprakasam A, Sivakumar V, Thirumarimurugan M (2015) Influencing parameters in the photocatalytic degradation of organic effluent via nanometal oxide catalyst: a review. *Indian Journal of Materials Science*, 2015,1-16.
- [18] Chen T, Zheng Y, Lin JM, Chen G (2008) Study on the photocatalytic degradation of methyl orange in water using Ag/ZnO as catalyst by liquid chromatography electrospray ion- trap mass spectrometry. *Journal of the American Society for Mass Spectrometry*, 19, 997-1003.
- [19] Awazu K, Fujimaki M, Rockstuhl C, Tominaga J, Murakami H, Ohki Y, Yoshida N, Watanabe T (2008) A plasmonic photocatalyst consisting of silver nanoparticles embedded in titanium dioxide. *Journal of the American Chemical Society*, 130, 1676-1680, <https://doi.org/10.1021/ja076503n>.
- [20] Yu T, Tan X, Zhao L, Yin Y, Chen P, Wei J (2010) Characterization, activity and kinetics of a visible light driven photocatalyst: cerium and nitrogen co-doped TiO₂ nanoparticles. *Chemical Engineering Journal*, 157, 86-92.
- [21] umar PSS, Raj MR, Anandan S (2010) Nanoporous Au-TiMCM-41-An inorganic hybrid photocatalyst toward visible photooxidation of methyl orange. *Solar Energy Materials and Solar Cells*, 94, 1783-1789.
- [22] Bechambi O, Najjar W, Sayadi S (2016) The nonylphenol degradation under UV irradiation in the presence of Ag-ZnO nanorods: effect of parameters and degradation pathway. *Journal of the Taiwan Institute of Chemical Engineers*, 60, 496-501.
- [23] Kaviyarasu K, Manikandan E, Nuru ZY, Maaza M (2015) Investigation on the structural properties of CeO₂ nanofibers via CTAB surfactant. *Materials Letters*, 160, 61-63.
- [24] Kaviyarasu K (2016) Photoluminescence of well-aligned ZnO doped CeO₂ nanoplatelets by a solvothermal route. *Materials Letters*, 183, 351-354,
- [25] Maria Magdalane C, Kaviyarasu K, Judith Vijaya J, Siddhardha B, Jeyaraj B (2017) Facile synthesis of heterostructured cerium oxide/yttrium oxide nanocomposite in UV light induced photocatalytic degradation and catalytic reduction: Synergistic effect of antimicrobial studies. *Journal of Photochemistry and Photobiology B: Biology* 173, 23-34.
- [26] Kasinathan K, Kennedy J, Elayaperumal M, Henini M, Malik M (2016) Photodegradation of organic pollutants RhB dye using UV simulated sunlight on ceria based TiO₂ nanomaterials for antibacterial applications. *Scientific Reports* 6, 38064.
- [27] Lee JC, Kim TG, Choi HJ, Sung YM (2008) Enhanced Photochemical Response of TiO₂/CdSe Heterostructured Nanowires Cryst.



- Growth Des. 8 750.
- [28] Banerjee S, Mohapatra SK, Das PP, Misra M (2008) Synthesis of Coupled Semiconductor by Filling 1D TiO₂ Nanotubes with CdS Chem. Mater. 20 6784.
- [29] Vogel R, Hoyer P, Weller H (1994) Application of heterogeneous photocatalysis in water contamination treatment J Phys Chem, 98: 3183
- [30] Kryukov AI, Kuehmii SYa, Pokhodenko VD (2000) Theor Exp Chem, 36: 63.
- [31] Akamatsu K, Takei S, Mizuhata M, Kajinami A, Deki S, Takeoka S, Fujii M, Hayashi S, Yamamoto K (2000) Preparation and characterization of polymer thin films containing silver and silver sulfide nanoparticles Thin Solid Films, 359: 55.
- [32] Hodes G, Manassen J, Cahen D (1976)
- [37] Xu Q, Wellia C, Sk DV, Lim MA, Loo KH, Liao JSC, Amal DW, Tan RY TT (2008) J. Photochem Photobiol, A, 210, 187.
- [38] Li G, Leung MKH (2010) Template-free synthesis of hierarchical porous SnO₂ J. Sol-gel Sci. Technol 53, 499.
- [39] Krishnakumar B, Subash B, Swaminathan M (2012) AgBr–ZnO – An efficient nanophotocatalyst for the mineralization of Acid Black 1 with UV light Sep. Purif. Technol 85, 35, <https://doi.org/10.1016/j.seppur.2011.09.037>.
- [40] Chen C, Li Z, Lin H, Wang G, Liao J, Li M, Lv S, Li W (2016) Enhanced visible light photocatalytic performance of ZnO nanowires integrated with CdS and Ag₂S Dalton Trans. 45, 3750, <https://doi.org/10.1039/C5DT04533A>.
- [41] Rajamanickam D, Shanthi M (2012) Photocatalytic degradation of an organic pollutant by zinc oxide-solar process, Arabian J. Chem, 9, 1858-1868, <https://doi.org/10.1016/j.arabjc.2012.05.006>.
- [42] Krishnakumar B, Selvam K, Velmurugan R, Swaminathan M (2010) Influence of Photoelectrochemical energy conversion and storage using polycrystalline chalcogenide electrodes Nature, 261: 403.
- [33] Kitova S, Eneva J, Panov A, Haefke H (1994) Infrared photography based on vapor-deposited silver sulfide thin films J Imaging Sci Technol, 38: 484.
- [34] Hull S, Keen DA, Sivia DS, Madden PA, Wilson M (2002) High Temperature Structural Study of Ag₂S J Phys Condens Matter, 14: L9.
- [35] Minami T (1987) Recent progress in superionic conducting glasses J Non-Cryst Solids, 95: 107.
- [36] Lei X, Xue X. & Yang H (2014) Preparation and characterization of Ag-doped TiO₂ nanomaterials and their photocatalytic reduction of Cr (VI) under visible light. Applied Surface Science, 321, 396-403. operational parameters on photomineralization of Acid Black 1 with ZnO, Desalin. Water Treat. 24, 132–139, <https://doi.org/10.5004/dwt.2010.1466>.
- [43] Subash B, Krishnakumar B, Swaminathan M, Shanthi M (2013) Photocatalytic performance of WO₃ loaded Ag–ZnO for Acid Black 1 degradation by UV-A light, J. Mol. Catal. A: Chem. 366, 54–63.
- [44] Krishnakumar B, Swaminathan M (2012) Photodegradation of Acid Violet 7 with AgBr–ZnO under highly alkaline conditions, Spectrochim Acta Part A 99, 160–165.
- [46] Subash B, Krishnakumar B, Velmurugan R, Swaminathan M, Shanthi M (2012) Synthesis of Ce co-doped Ag–ZnO photocatalyst with excellent performance for NBB dye degradation under natural sunlight illumination, Catal. Sci. Technol. 2, 2319–2326, <https://doi.org/10.1039/C2CY20254A>.
- [47] Subash B, Krishnakumar B, Swaminathan M, Shanthi M (2013) Highly efficient, solar active and reusable photocatalyst, Zr loaded Ag–ZnO for reactive red 120 dye



- degradation with synergistic effect and dye sensitized mechanism, *Langmuir* 29 939–949,
<https://doi.org/10.1021/la303842c>.
- [48] Kuzhalosai V, Subash B, Senthilraja A, Dhatshanamurthi P, Shanthi M (2013) Synthesis, Characterization and photocatalytic properties of SnO₂–ZnO composite under UV-A light, *Spectrochim Acta Part A* 115, 876–882, <https://doi.org/10.1016/j.saa.2013.06.106>.
- [49] Okamoto K, Yamamoto Y, Tanaka H, Itaya A (1985) Heterogeneous Photocatalytic Decomposition of Phenol over TiO₂ Powder *Bull. Chem.Soc. Jpn*, 58,
- [53] Tang WZ, An H (1995) Photocatalytic degradation kinetics and mechanism of acid blue 40 by TiO₂/UV in aqueoussolution *Chemosphere*, 31, 4171.
- [54] Chem LC, Chou TC (1993) *J. Mol. Catal*, 85, 201.
- [55] Wenhua L, Hong L, Suoan C, Jianqing Z, Chunan (2000) *J. Photochem. Photobiol. A*, 131, 125.
- [56] Alaton IA, Balcioğlu IA (2001) Photochemical and heterogeneous photocatalytic degradation of waste vinylsulphone dyes: a case study with hydrolyzed Reactive Black 5 *J. Photochem. Photobiol. A*, 14.
- [57] Sharma A, Rao P, Mathur RP, Ametha SC (1995) *J. Photochem. Photobiol. A*, 86, 197.
- 2015.
- [50] A, Plaidy O (1995), Assessment of the importance of the role of H₂O₂ and O₂^{•-} in the Photocatalytic degradation of 1,2-dimethoxybenzene *Sol. Energy Mater. Sol. Cells*, 38, 391.
- [51] Bekholet M, Lindner M, Weichgrebe D, Bahnemann DW (1996) *Sol. Energy*, 56, 455.
- [52] Pelizzetti E, Carlin V, Minero C, Gratzel M (1991) Enhancement of the rate of photocatalytic degradation on TiO₂ of 2-chlorophenol, 2,7-dichlorodibenzodioxin and atrazine by inorganic oxidizing species *New J. Chem*, 15, 351.